



HAL
open science

Photoinitiation behavior of phenothiazines containing two oxime ester functionalities (OXEs) in free radical photopolymerization and 3D printing application

Yijun Zhang, Fabrice Morlet-Savary, Michael Schmitt, Bernadette Graff, Alexandre Rico, Malika Ibrahim-Ouali, Frédéric Dumur, Jacques Lalevée

► To cite this version:

Yijun Zhang, Fabrice Morlet-Savary, Michael Schmitt, Bernadette Graff, Alexandre Rico, et al.. Photoinitiation behavior of phenothiazines containing two oxime ester functionalities (OXEs) in free radical photopolymerization and 3D printing application. *Dyes and Pigments*, 2023, 215, pp.111202. 10.1016/j.dyepig.2023.111202 . hal-04038627

HAL Id: hal-04038627

<https://hal.science/hal-04038627v1>

Submitted on 21 Mar 2023

HAL is a multi-disciplinary open access archive for the deposit and dissemination of scientific research documents, whether they are published or not. The documents may come from teaching and research institutions in France or abroad, or from public or private research centers.

L'archive ouverte pluridisciplinaire **HAL**, est destinée au dépôt et à la diffusion de documents scientifiques de niveau recherche, publiés ou non, émanant des établissements d'enseignement et de recherche français ou étrangers, des laboratoires publics ou privés.

Photoinitiation Behavior of Phenothiazines Containing Two Oxime Ester Functionalities (OXEs) in Free Radical Photopolymerization and 3D Printing Application

Yijun Zhang,^{†,‡} Fabrice Morlet-Savary,^{†,‡} Michael Schmitt,^{†,‡} Bernadette Graff,^{†,‡} Alexandre Rico,[§] Malika Ibrahim-Ouali,^α Frédéric Dumur,^{§,*} and Jacques Lalevée^{†,‡,*}

[†] Université de Haute-Alsace, CNRS, IS2M UMR 7361, F-68100 Mulhouse, France

[‡] Université de Strasbourg, France

[§] Aix Marseille Univ, CNRS, ICR, UMR 7273, F-13397 Marseille, France

^α Aix Marseille Univ, CNRS, Centrale Marseille, iSm2, F-13397 Marseille, France

Abstract

Twelve type I photoinitiators (PIs) containing two oxime esters functionalities on the terminal moiety were synthesized. These OXEs have high light absorptivities in the visible range, and some of them showed better photoinitiation abilities than the commercial photoinitiator diphenyl(2,4,6-trimethylbenzoyl)phosphine oxide (TPO), under the irradiation of a 405 nm LED. Photoinitiation mechanisms of these OXEs are proposed through theoretical calculations, the detection of CO₂, and the ESR investigation of the free radical generation. 3D Objects could be manufactured successfully by using the most reactive OXEs as photoinitiators with a stereolithographic 3D printer. In addition, these reactive OXEs also displayed a thermal initiation behavior, meaning that these OXEs can served as thermal or photochemical initiators.

Introduction

Photopolymerization of bulk materials has known a rapid development during the last decades, benefiting from its unique characteristics, including high reaction rates, good spatial control and mild reaction conditions (room temperature, absence of organic solvents), and low-energy consumption.¹⁻³ Therefore, photopolymerization can be used in different fields ranging from traditional to high-precision industries, such as

coatings, inks, microelectronics, biomedicine, and 3D printing.^{2, 4-6} To get a polymerization process, three elements have to be considered : the light source used for irradiation, the photoinitiating system used for the generation of active initiating species, and the monomer/oligomer which is in its liquid state.⁷⁻⁹ Light-emitting diodes (LEDs) have become one of the most popular light sources in photopolymerization due to their intrinsic advantages including low energy consumption, fewer harmful UV rays, lower heat generation, longer lifetime, compactness and lightweight.^{10, 11} In order to match the emission of LEDs, photoinitiating systems should exhibit high light absorptivity and high photoreactivity in the emission range of the light sources.¹²⁻¹⁴ Many new multicomponent photoinitiating systems have been developed and reported in recent years.¹⁵⁻¹⁸ However, most of these photoinitiating systems suffer from the same drawbacks, namely a decrease of the initiating ability particularly in highly viscous resins due to difficult interactions between the photosensitizers and the different additives.¹⁹ Therefore, the development of type I photoinitiators becomes a desirable way attracting more and more attention from researchers. By developing monocomponent systems, the direct cleavage process upon photoexcitation of a selected bond in order to generate active free radicals for photopolymerization constitutes an appealing strategy. In addition, the other interesting way is to develop nanoparticle-basic systems for photoinitiation in photopolymerization, such as Zinc oxide (ZnO).^{20, 21}

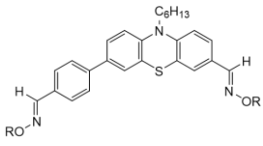
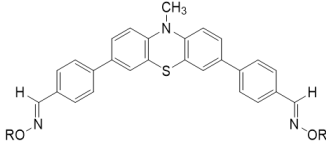
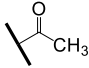
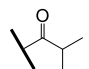
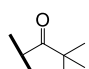
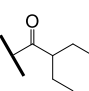
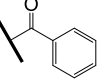
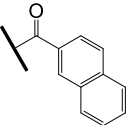
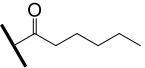
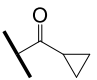
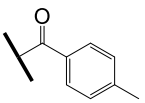
Oxime esters (OXEs) are a family of compounds capable to undergo a homolytic cleavage of a N-O bond upon photoexcitation, generating radicals.²²⁻²⁴ Normally, the N-O bond can cleave upon light irradiation to generate iminyl and acyloxy/aryloxy radicals.^{25, 26} If iminyl radicals are unreactive for polymerization, conversely, active free radicals can be formed by decarboxylation of acyloxy/aryloxy radicals subsequent to photocleavage, resulting in the release of CO₂ in the reaction medium.²⁷ Interest of these structures also relies in the fact that subsequent to the irreversible decarboxylation reaction, the resulting radicals are unable to recombine with iminyl radicals so that the resulting alkyl or aryl radicals can only contribute to polymerization. At present, there are only few benchmark photoinitiators based on the oxime ester structure. To illustrate

this, only *O*-benzoyl- α -oxo oxime and *O*-acetyloxime used for pigmented formulations are commercially available.²⁸ However, these compounds can only be photoexcited around 330 nm, which means that these structures exhibit low performances when excited in the near-UV range or with visible light. **This constatation shows that there is an urgent need to develop new oxime ester-based photoinitiators with high light absorption capacity and photo-reactivity in the near UV/visible range.**

In our previous works, **different types of oxime esters were developed**, including chromophores such as nitrocarbazoles, triphenylamines, coumarins, pyrenes and anthracenes, naphthalenes were used to design OXEs.^{25, 29-32} In the literature, many other types of OXEs were reported by other research groups, and chalcones, coumarins, bicarbazoles, phenothiazines, stilbenes, phenyl thienyl thioethers and fluorophenyl-based OXEs can be cited as other examples of oxime esters.^{19, 24, 27, 33-37} All of these photoinitiators contained only one oxime ester group, and the different structures showed favorable cleavage process and decarboxylation reaction. Therefore, in order to develop new OXEs that could exhibit a higher photoinitiation ability than the aforementioned structures, the synthesis of photoinitiators containing two OXE functionalities as end groups are proposed and their photoinitiating ability examined.³⁸

In this work, we successfully synthesized twelve phenothiazine-based initiators containing two OXE functionalities as end groups, and chemical structures of the different OXEs are listed in Scheme 1. UV-visible absorption properties, fluorescence spectra, fluorescence lifetimes, free radical photopolymerization and electron spin resonance spin trapping (ESR-ST) experiments were performed to estimate their photopolymerization behaviors upon visible light irradiation. Mechanism of photoinitiation was also examined in detail. Finally, 3D printing experiments and thermal polymerization were carried out on the three formulations with the highest photoinitiating efficiencies.

Scheme 1. Chemical Structures of the 12 Investigated OXEs.

R		
		
H	OXE-A0	OXE-B0
	OXE-A1	OXE-B1
	OXE-A2	OXE-B2
	OXE-A3	OXE-B3
	/	OXE-B4
	/	OXE-B5
	/	OXE-B6
	/	OXE-B7
	/	OXE-B8
	/	OXE-B9

Experimental Section

Synthesis of OXEs

Synthetic procedures used to access to the different structures OXE-A0-OXE-A3, OXE-B0-OXE-B9 are depicted in detail in SI.

Other Materials

Trimethylolpropane triacrylate (TMPTA) used as the monomer for free radical photopolymerization (RFP) was purchased from Allnex (Ivry sur Seine, France). **The storage inhibitor was not removed.** Diphenyl (2,4,6-trimethylbenzoyl) phosphine oxide (TPO) was purchased from Lambson Ltd. (United Kingdom). *N-tert*-Butyl- α -phenylnitron (PBN), used as the free radical trapping agent, was obtained from TCI-Europe (Paris, France). The colloidal silica suspension (LUDOX AS 30, 30 wt % suspension in H₂O) was obtained from Sigma-Aldrich.

UV-Visible Absorption Properties

UV-Visible absorption spectra of OXEs dissolved in acetonitrile were obtained with a JASCO V30 spectrometer (**1 cm optical path length**). Steady-state photolysis of OXEs dissolved in acetonitrile was performed using a JASCO V30 spectrometer, under irradiation with a 405 nm LED (110 mW·cm⁻²). Concentration of OXEs was controlled at 5×10⁻⁵ M in acetonitrile as solvent for both UV-Visible absorption and steady-state photolysis experiments.

Fluorescence Spectra and Fluorescence Lifetime

Fluorescence spectra of OXEs (concentration in the range of 5×10⁻⁵ M in acetonitrile as solvent) were investigated on a JASCO FP-750 spectrofluorometer. Fluorescence excited-state lifetimes were determined with a HORIBA PPD-850 detector. The impulse response function (IRF) of the apparatus was evaluated through the colloidal silica suspension LUDOX, and the excitation wavelength was set at 367 nm and the pulse duration was shorter than 1.4 ns.

Singlet excited-state energies (E_{S1}) of OXEs were calculated from the intersection of the normalized fluorescence emission spectra and the normalized UV-vis absorption spectra (see Figure 4, Figure S6 and Figure S7) and E_{S1} was calculated by equation (1). Enthalpies of the cleavage process of the N-O bond ($\Delta H_{\text{Cleavage}}$) from OXEs were calculated by equation (2) and equation (3), based on the energies of the singlet or triplet excited states (E_{S1} or E_{T1}) and the dissociation energies of the N-O bond (BDE).

$$E_{S1} = 1240 / \text{Wavelength of intersection} \quad \text{equation (1)} \quad \Delta H_{\text{Cleavage}_{S1}} =$$

$$BED_{(N-O)} - E_{S1} \quad \text{equation (2)}$$

$$\Delta H_{\text{Cleavage}_{T1}} = BED_{(N-O)} - E_{T1} \quad \text{equation (3)}$$

Free Radical Photopolymerization

Firstly, the different OXEs and the monomer (i.e. TMPTA) were mixed in a glass bottle and stirred overnight away from light. The concentration of OXEs in all formulations was controlled at 1×10^{-5} mol.g⁻¹ in TMPTA, which corresponds to a weight percentage in the range of 0.45 wt% to 0.76 wt% in TMPTA depending on their different molecular masses. In order to reduce or avoid the oxygen inhibition, drops of the homogenous formulation were deposited in the laminate between two transparent polypropylene films and the thickness was in the range of 25 µm. For thick sample (1.4 mm), the formulation was deposited in a plastic mold. After, the free radical photopolymerization kinetics of TMPTA upon exposure to a 405 nm LED (110 mW.cm⁻²) at room temperature for 800 s were investigated by a real-time Fourier transformed infrared (RT-FTIR) spectroscopy (JASCO FTIR-4100). The acrylate characteristic peak area of TMPTA for thin sample was selected from 1589 to 1665 cm⁻¹. And that of TMPTA for thick sample was in the near-infrared range at ~6160 cm⁻¹. The acrylate function conversion (FC) of TMPTA for a given time was calculated by equation 3:

$$FC(t) = (A_0 - A_t) / A_0 \times 100\% \quad \text{equation (3)}$$

Where A_0 and A_t are the peak area at $t = 0$ s and at any t respectively. The final acrylate conversion was determined by the shape of the conversion curves, which is reached either after a plateau is reached (rate practically zero even under illumination) or after a certain illumination period.

Electron Spin Resonance Spin Trapping (ESR-ST)

ESR-spin trapping experiments were performed with a X-band spectrometer (Bruker EMX plus). N₂ saturated PBN was selected as the free radical trapping agent, and the concentration of PI dissolved in PBN was controlled at 5×10^{-5} M. During ESR-

Commenté [MS1]: Define and add the solvent

Commenté [f2R1]: Generally tert-butyl benzene ; PBN stands for N-tert-Butyl-α-phenylnitron ; CAS : 3376-24-7, from TCI chemicals, Japan

ST experiments, PBN solvent containing PI was irradiated upon 405 nm LED (110 mW·cm⁻²) at room temperature. ESR spectra simulations were performed by WINSIM software.

3D Printing with Light

Concentration of OXEs in 3D printing formulations was controlled at 1×10⁻⁵ mol.g⁻¹ in TMPTA. The 3D objects were manufactured by a 3D printer (Moai 130, from Peopoly), based on stereolithography (SLA). The slot size of the device is 9.5cm*6.5cm*1.0cm (length, width and height) and the layer thickness was controlled at 0.02 mm. The laser spot size is 70 μm and its power was set at 90 mW. Direct Laser write (DLW) experiments were also performed with a laser diode (405 nm, supplied from Thorlabs, UK), and the slot was a homemade glass tank (2 mm thickness). The laser intensity was 110 mW and the spot size was 50 μm.

Thermal Initiating Behavior

Differential scanning calorimetry (DSC) was performed to analyze the thermal initiation performance of OXEs (1×10⁻⁵ mol.g⁻¹ in TMPTA) by a Mettler Toledo DSC (10 °C.min⁻¹ from 20 to 250 °C, under nitrogen). According to the heat release value of acrylate double bond at 78.61 kJ.mol⁻¹ in thermal polymerization, the function conversion of TMPTA in thermal polymerization can be calculated with the equation (4):

$$FC = \text{Heat released} / 795.9 \times 100\% \quad \text{equation (4)}$$

Results and Discussion

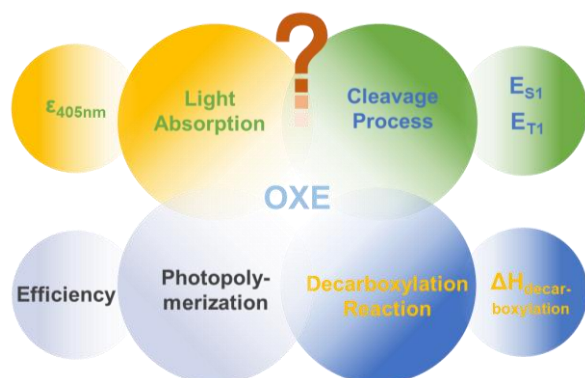
Strategy for the Molecular Design of OXEs

As shown in Scheme 2, there are many parameters affecting the photopolymerization efficiency, including light absorption, excited state cleavage, decarboxylation reaction and reactivity of the generated radicals.³⁹ In order to be efficient in photopolymerization upon the irradiation of 405 nm LED, the new OXEs should have an efficient light absorption around 405 nm, so that the maximum wavelength of absorption (λ_{max}), the molar extinction coefficients at maximum absorption wavelength (ϵ_{max}) and the molar extinction coefficients at 405 nm ($\epsilon_{405\text{nm}}$)

Commenté [MS3]: Within the cavity of the ESR device ?

Commenté [f4R3]: Generally sample is irradiated inside the cavity of the ESR apparatus, and the spectrum is recorded after light irradiation. This is the case, here

are important parameters. The N-O bond for OXEs must have an efficient cleavage process to obtain a good type I photoinitiator. As OXEs normally react from their singlet excited states (S_1) or triplet excited states (T_1), energies of the singlet or triplet excited states (E_{S_1} or E_{T_1}) and the dissociation energies of the N-O bond (BDE) were computed to check whether the reaction is favorable ($\Delta H < 0$). For free radical photopolymerization initiated by OXEs, the active free radicals are generated from the decarboxylation after cleavage process, which is a very important process for OXEs used as photoinitiators. After considering the light absorption properties and the cleavage and decarboxylation reactions, free radicals should be efficient for initiating photopolymerization, which can be indicated by final conversion of C=C double bond.



Scheme 2. Summary of the computable and measurable parameters governing the reactivity of OXE.

According to the parameters mentioned above, energy levels and contour plots of the Highest Occupied Molecular Orbital (HOMO) and the Lowest Unoccupied Molecular Orbitals (LUMO) of OXEs were calculated (see Scheme S1, S2 and S3). The electronic clouds of all OXEs are mainly distributed on the phenothiazine core and the oxime ester groups, and the bond dissociation energies of N-O bond (BDE) and the triplet excited-state energy (E_{T_1}) are listed in Table 4. As calculated by equation 3, $\Delta H_{\text{Cleavage } T_1} < 0$ is favorable for the N-O bond cleavage.

Light Absorption Property

UV-visible absorption spectra of OXEs are shown in Figure 1 and Figure S1, and the light absorption properties of all OXEs with different functional groups are listed in

Table 1. As shown in Figure S2 and Figure S3, **most of OXEs were well** dissolved in acetonitrile at room temperature, and the **solutions** of OXE-B3, OXE-B5, OXE-B6 OXE-B8 and OXE-B9 were cloudy, which **indicates** poor solubilities in acetonitrile. Therefore, ϵ_{\max} and $\epsilon_{405\text{nm}}$ of these five samples are not investigated.

Excluding those OXEs due to poor solubilities, other OXEs showed a broad light absorption band tailing up to 475 nm. In the series of OXE-A, the maximum absorption wavelength (λ_{\max}) of OXE-A1, OXE-A2 and OXE-A3 were located at **376, 372 and 372 nm** respectively. Compared to OXE-A0 (**with an absorption maximum around 360 nm**) that is not an oxime ester (**only an oxime N-OH group**), a red-shift of λ_{\max} of the three compounds could be detected for the oxime esters as shown in Figure 1.a, and this bathochromic shift can be explained by the presence of oxime ester groups acting as an electron-withdrawing group. A similar behavior can also be observed in the series of OXE-B. As shown in Table 1, compared to ϵ_{\max} of OXE-A0 (360 nm, $8700 \text{ M}^{-1} \cdot \text{cm}^{-1}$), OXE-A1, OXE-A2 and OXE-A3 all have larger ϵ_{\max} values (13100 , 12800 and $11100 \text{ M}^{-1} \cdot \text{cm}^{-1}$, respectively), and the same trend is also **observed** for the second series of OXEs, namely the series of OXE-B. Furthermore, the $\epsilon_{405\text{nm}}$ values of the OXE-A series (OXE-A1, OXE-A2 and OXE-A3) or the OXE-B series (OXE-B1, OXE-B2, OXE-B4 and OXE-B7) are larger than that of OXE-A0 or OXE-B0 respectively. Therefore, these results indicate that these OXEs can be more sensitive to light irradiation at 405 nm.

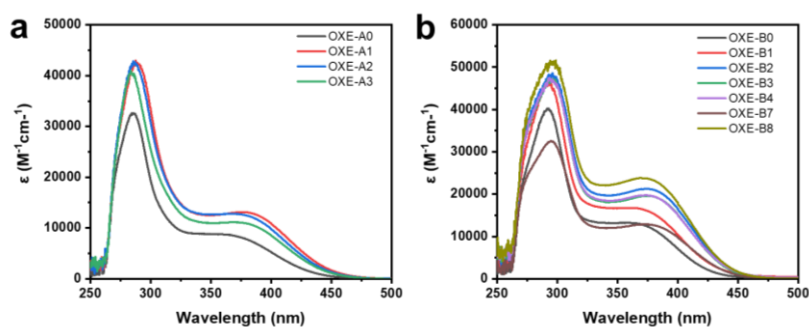


Figure 1. UV-visible absorption spectra of oxime ester derivatives in acetonitrile.

Table 1. Light absorption properties of OXEs.

OXE	λ_{\max} (nm)	ϵ_{\max} ($M^{-1} \text{ cm}^{-1}$)	$\epsilon_{405\text{nm}}$ ($M^{-1} \text{ cm}^{-1}$)
OXE-A0	360	8700	4500
OXE-A1	375	13100	9800
OXE-A2	369	12800	8700
OXE-A3	370	11100	7600
OXE-B0	362	13100	5800
OXE-B1	363	16700	8800
OXE-B2	370	21200	14500
OXE-B3	370	*	*
OXE-B4	370	19700	13200
OXE-B5	369	*	*
OXE-B6	368	*	*
OXE-B7	370	12800	8600
OXE-B8	369	*	*
OXE-B9	364	*	*

*: According on the low solubility in acetonitrile, ϵ_{\max} and $\epsilon_{405\text{nm}}$ were not investigated.

Steady-State Photolysis

Steady-state photolysis experiments were performed upon irradiation with a 405 nm LED to investigate the photolysis behaviors during light absorption (see Figure 2 and Figure S3). As shown in Figure 2, OXE-A0 and OXE-B0 both do not have an obvious decline after irradiation with a 405 nm LED for 120 s, which means that OXE-A0 and OXE-B0 are unable to initiate any photocleavage. Interestingly, the absorbance intensities of OXE-A1 (375 nm), OXE-B2 (370 nm) and OXE-B4 (370 nm) all have a rapid decline after 10 s of exposure to a 405 nm LED. Then, the absorptions decline gradually with increasing the irradiation time, which can be related to the homolytic cleavage of the N-O bond. Furthermore, the absorbance intensities of OXE-B2 and OXE-B4 at 350 nm exhibit a significant increasing trend, and this increase of absorption can be assigned to the fact that new photoproducts are formed upon irradiation, these compounds being issued from the photodecomposition of OXE-B2 and OXE-B4 after

photocleavage of the N-O bond. Steady-state photolysis spectra of all the other OXEs are shown in Figure S4 and S5. Noticeably, a decline of the absorption intensity of OXEs at their maximum absorption wavelength could be detected upon irradiation at 405 nm.

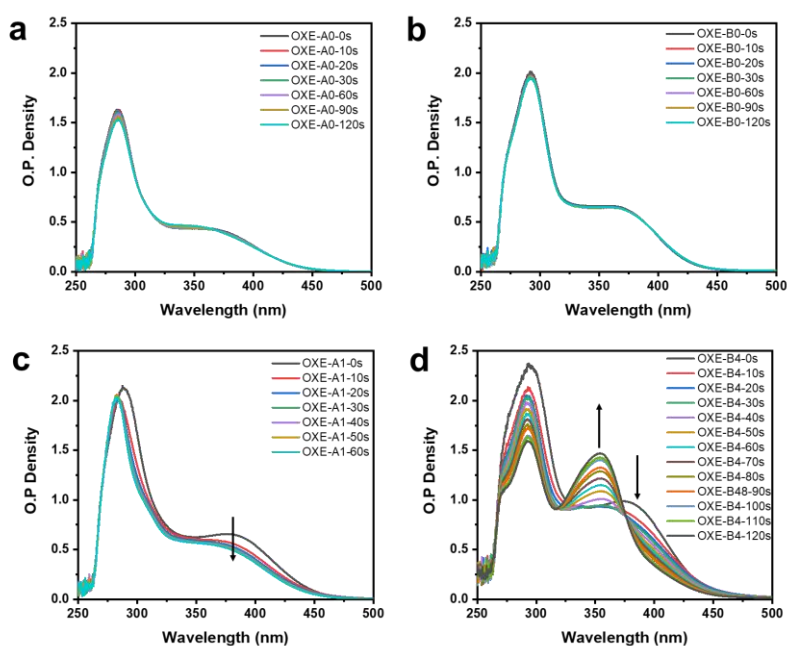


Figure 2. Steady-state photolysis of OXEs in acetonitrile upon irradiation with a 405 nm LED. (a) OXE-A1 and (b) OXE-B4.

The singlet excited-state energies (E_{S1}) of OXEs were obtained from the intersection of their fluorescence emission spectra and their UV-visible absorption spectra (see Figure 3, Figure S6 and Figure S7). When the $\Delta H_{\text{Cleavage } S1}$ values are negative ($\Delta H_{\text{Cleavage } S1} < 0$), it indicates that photocleavage of the N-O bond from the singlet excited state is favorable. As shown in Tables 3 and 4, all OXEs have favorable $\Delta H_{\text{Cleavage } S1}$ for cleavage, excepted OXE-A0 and OXE-B0 that are not oxime esters and for which the cleavage of the N-OH bond is totally unfavorable. Furthermore, excited state lifetimes of OXEs could be measured (see Figure 3, Figure S8 and Figure S9), and the lifetime values are listed in Table 3. Normally, OXEs

with a high initiating efficiency have a short excited state lifetime, which also can be beneficial for the cleavage process. In addition, the negative $\Delta H_{\text{Cleavage T1}}$ values also suggests the cleavage process of the N-O bond to be favorable.

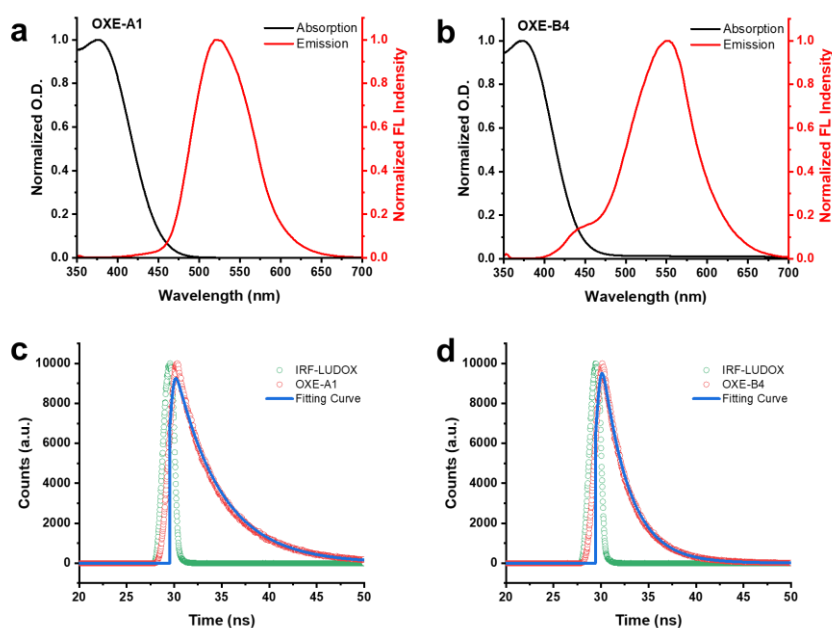


Figure 3. Singlet-state energy determination of (a) OXE-A1 and (b) OXE-B4, and fluorescence decay curve of (c) OXE-A1 and (d) OXE-B4.

Table 3. N-O BED, E_{S1} , E_T , $\Delta H_{\text{Cleavage S1}}$, $\Delta H_{\text{Cleavage T1}}$ and lifetime of the series OXE-A.

Pis	N-O BDE		E_{S1} (kcal mol ⁻¹)	$\Delta H_{\text{Cleavage S1}}$ (kcal mol ⁻¹)	E_T (kcal mol ⁻¹)	$\Delta H_{\text{Cleavage T1}}$ (kcal mol ⁻¹)	Lifetime (ns)
	R ₁ or R ₂	(kcal mol ⁻¹) 1)					
OXE-A0	R ₁	65.21	63.01	2.20	53.35	11.86	4.16
	R ₂	65.17		2.16		11.82	
OXE-A1	R ₁	48.50	63.39	-14.80	52.03	-3.53	4.91
	R ₂	48.76		-14.65		-3.27	

OXE-A2	R ₁	48.20	63.27	-15.07	53.99	-5.79
	R ₂	48.23		-15.04		-5.76
OXE-A3	R ₁	47.50	64.04	-16.54	53.94	-6.44
	R ₂	47.52		-16.52		-6.42

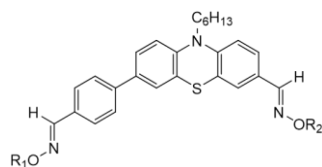
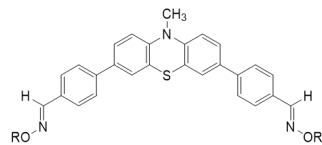


Table 4. N-O BDE, E_{S1}, E_T, ΔH_{Cleavage S1}, ΔH_{Cleavage T1} and lifetime of the series OXE-B.

Pis	N-O BDE (kcal mol ⁻¹)	E _{S1} (kcal mol ⁻¹)	ΔH _{Cleavage S1} (kcal mol ⁻¹)	E _T (kcal mol ⁻¹)	ΔH _{Cleavage T1} (kcal mol ⁻¹)	Lifetime (ns)
OXE-B0	65.22	63.52	1.7	53.03	12.19	3.31
OXE-B1	48.92	65.68	-16.76	54.00	-5.08	3.55
OXE-B2	48.24	66.46	-18.22	53.97	-5.73	2.95
OXE-B3	47.54	66.01	-18.47	53.92	-6.38	3.01
OXE-B4	46.84	66.28	-19.44	54.02	-7.18	2.95
OXE-B5	48.15	63.85	-15.7	53.72	-5.57	1.75
OXE-B6	48.05	67.72	-19.67	53.69	-5.64	3.2
OXE-B7	47.73	66.20	-18.47	53.37	-5.64	3.00
OXE-B8	47.66	67.32	-19.66	54.02	-6.36	2.81
OXE-B9	47.90	67.07	-19.17	53.74	-5.84	2.64



Free Radical Photopolymerization

Photopolymerization experiments of TMPTA containing these different OXEs (1×10^{-5} mol.g⁻¹, 0.45-0.76 wt% depending on their different molecular masses) or the

commercial photoinitiator TPO ($1 \times 10^{-5} \text{ mol.g}^{-1} = 0.35 \text{ wt\%}$) were investigated to evaluate their photoinitiation abilities.

Photopolymerization profiles in thin samples are presented in Figure 2 and the final conversions (FCs) of the different formulations are listed in Table 5. As shown in Figure 2, OXE-A1 (80%), OXE-B2 (74%) and OXE-B4 (66%) have the best photoinitiation abilities in their respective series during the polymerization of thin samples. Their FC values are also larger than those of the TPO-containing formulation (65.0%), demonstrating their good initiation performance.

Photopolymerization profiles of thick samples with different formulations are presented in Figure S10 in which OXE-A1, OXE-B2 and OXE-B4 based systems still show favorable performances. It is also interesting to note that OXE-B1 and OXE-B6 could not initiate efficient photopolymerizations. These counter-performances can be assigned to the low efficiency of the cleavage process and the decarboxylation reaction for OXE-B1 (see Figure S12.b and Figure S13), and the poor efficiency of the decarboxylation reaction for OXE-B6 (see Figure S8.i). In addition, containing the same R group as OXE-B1, OXE-A1 has better photoinitiation abilities on both thin and thick samples, which shows the position R2 of OXE-A1 might be more favorable.

In our previous work,^{29,40} the best monomer conversions obtained during the FRP of TMPTA for resin containing monofunctional OXEs i.e. dyes comprising only one oxime ester group were between 64 and 68%, with concentrations of $2 \times 10^{-5} \text{ mol.g}^{-1}$ in TMPTA for the different OXEs. Interestingly, comparable or higher FCs could be successfully obtained in this work, for OXE concentrations of only $1 \times 10^{-5} \text{ mol.g}^{-1}$ in TMPTA. Considering that difunctional OXEs were used, the concentration used in this work is therefore twice lower than that used in the previous work. Nevertheless, even with a twofold reduction of the concentration, higher final monomer conversions were obtained. It therefore demonstrates the higher photoinitiating ability of the newly developed difunctional OXEs. In addition, some of these OXEs also showed good performances for the polymerization of thick samples (1.0 mm), (i.e., OXE-A1, OXE-B2 and OXE-B4), what is remarkable. Consequently, according to the FCs obtained

Commenté [MS5]: What about A1? It can be assumed due to the fact that A1 contains the same R groups that the position R2 might be more favorable / reactive.

Commenté [ZY6R5]: I think the other reason could be the transmission of light or the color of the formulation, because OXE-B1 has a darker color than other OXEs.

during the FRP of TMPTA, OXEs containing two oxime ester groups exhibit improved photoinitiation efficiencies than the monofunctional ones.

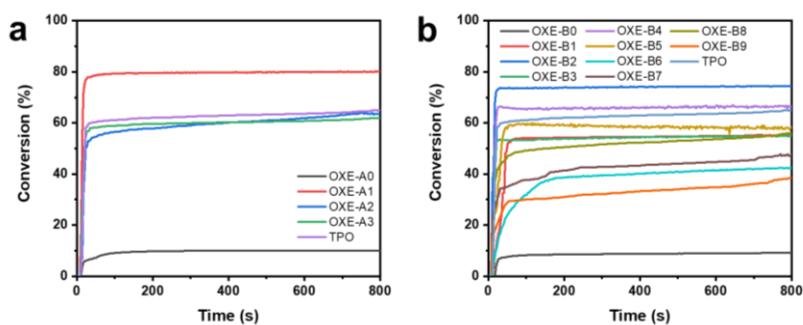


Figure 4. Photopolymerization profiles of TMPTA in laminate ($\sim 25 \mu\text{m}$) upon exposure to a 405 nm LED in the presence of different OXEs ($1 \times 10^{-5} \text{ mol.g}^{-1}$ in TMPTA) and the commercial photoinitiator TPO. The irradiation starts at $t = 10 \text{ s}$.

Table 5. Final Function Conversions (FCs) of TMPTA Containing Different OXEs.

OXE	Final Conversion (FC, %)
OXE-A0	11
OXE-A1	80
OXE-A2	64
OXE-A3	62
OXE-B0	9
OXE-B1	55
OXE-B2	74
OXE-B3	55
OXE-B4	66
OXE-B5	58
OXE-B6	42
OXE-B7	48
OXE-B8	56
OXE-B9	39
TPO	65

Decarboxylation Reaction

For OXEs based photoinitiation systems, the decarboxylation reaction take place after a homolytic cleavage of the N-O bond upon irradiation and can form free radicals after release of CO₂. In this work, the decarboxylation reaction was investigated by monitoring the generation of CO₂, which can easily be detected by RT-FTIR (see Figure 5, Figure S11 and Figure S12). As shown in Figure 5.a and 5.b, the appearance of the CO₂ absorbance peak can be detected for numerous OXEs at 2337 cm⁻¹ during photopolymerization. This phenomenon can be observed for most of the OXE/TMPTA systems, excepted with OXE-B1, OXE-B5, OXE-B6 and OXE-B9, for which clear evidence that the decarboxylation reaction for these OXEs does not occur was provided. In previous works, our group has reported a series of enthalpy of decarboxylation reaction ($\Delta H_{\text{decarboxylation}}$) and demonstrated that when the $\Delta H_{\text{decarboxylation}}$ was negative, the decarboxylation process was favorable.³¹ As previously reported, these values for benzene acyl group, a naphthalene acyl group and a benzyloxy group are 5.92, 6.24 and 6.92 kcal mol⁻¹ respectively, which means these corresponding OXEs (OXE-B5, OXE-B6 and OXE-B9) are less favorable for decarboxylation reaction. This may explain why the CO₂ peak during photopolymerization cannot be observed in these three OXE/systems. Interestingly, the CO₂ peak in OXE-B1/TMPTA system is difficult to be observed, and this will be discussed below in the section of ESR.

As shown in Figure 5.c, the absorbances of CO₂ in OXE-A1 and OXE-B4 increase rapidly from t = 10 s to t = 60 s, related to the generation of CO₂ by the decarboxylation reaction. After t = 60 s, the absorbances of CO₂ start to decrease which may be due to the diffusion from the cured samples to the air. This trend is in agreement with their acrylate function conversions, which increase rapidly accompanied by the generation of CO₂ for the OXE-A1/TMPTA and OXE-B4 systems from t = 10 s to t = 60 s. This behavior can be observed in the other OXE/TMPTA systems, such as OXE-B2/TMPTA (see Figure S13).

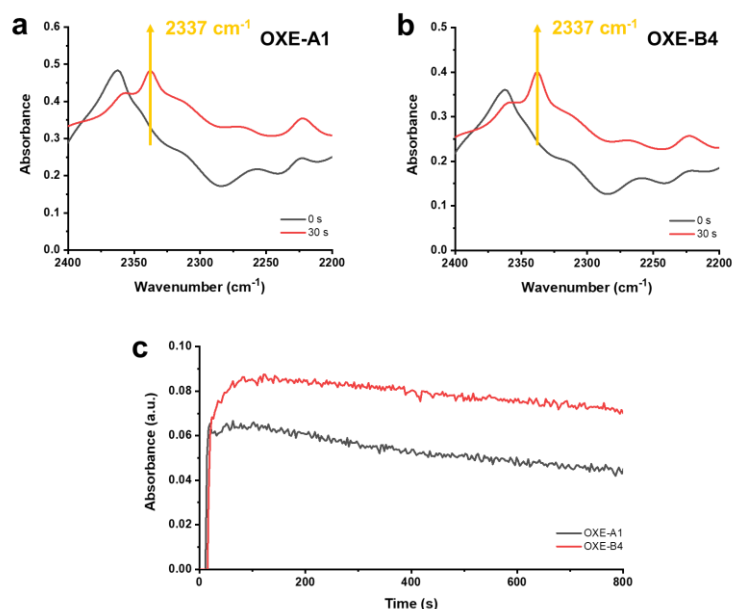


Figure 5. Infrared spectra of (a) OXE-A1 in TMPTA and (b) OXE-B4 in TMPTA at $t = 10$ and 30 s, and (c) the absorption intensity of CO₂ obtained from the OXE-A1/TMPTA and OXE-B4/TMPTA systems respectively.

Electron Spin Resonance Spin Trapping (ESR-ST)

Besides the generation of CO₂, the active radical is another product in the decarboxylation reaction. Here, ESR-ST was carried on OXE-A1, OXE-B1, OXE-B2 and OXE-B4 (see Figure 6 and Figure S14), and two kinds of radicals (alkyl-COO[•] and alkyl radical) were trapped by PBN in each system after 405 nm irradiation. For OXE-A1 system, the values of the hyperfine coupling constants for alkyl-COO[•] (72.1%) are $\alpha_N = 13.5$ G and $\alpha_H = 1.8$ G, which can be assigned to the acetyl radical (CH₃COO[•]). The value of hyperfine coupling constants of the second alkyl radical (27.9%) were $\alpha_N = 13.6$ G and $\alpha_H = 4.8$ G, and it could be the methyl radical. For OXE-B2, the values of hyperfine coupling constants are $\alpha_N = 13.7$ G and $\alpha_H = 1.7$ G, which can be assigned to the isobutyryl radical (83.8%), and the second radical could be isopropyl radical (16.2%, $\alpha_N = 13.7$ G and $\alpha_H = 4.8$ G) generated from the decarboxylation reaction of the isobutyryl radical. For OXE-B4, the values of hyperfine coupling constants are $\alpha_N = 13.7$ G and $\alpha_H = 1.6$ G, which can be assigned to the isocaproyl radical (68.0%), and

the second radical could be isopentyl radical (32.0%, $\alpha_N = 13.7$ G and $\alpha_H = 4.6$ G) generated from the decarboxylation reaction of the isobutyryl radical. The ESR-ST for OXE-B1 was also carried out, and there are no obvious signals being observed (see Figure S14). This means neither cleavage process nor decarboxylation reaction of OXE-B1 are efficient, which corresponds to the results of related photopolymerization result (low final conversion in Figure 4.b) and the detection of CO₂ (see Figure S12.c).

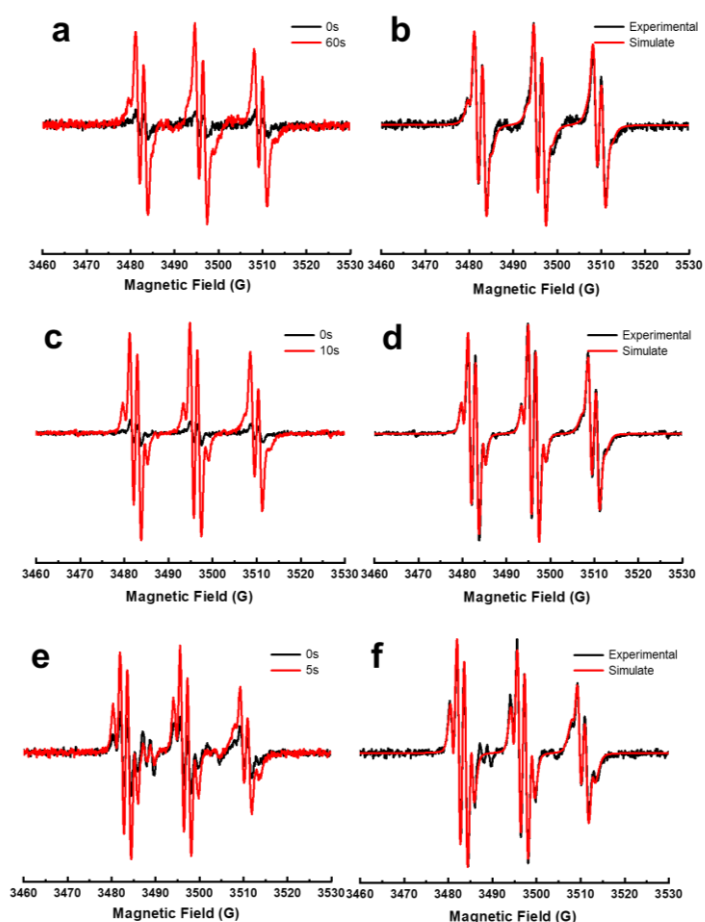
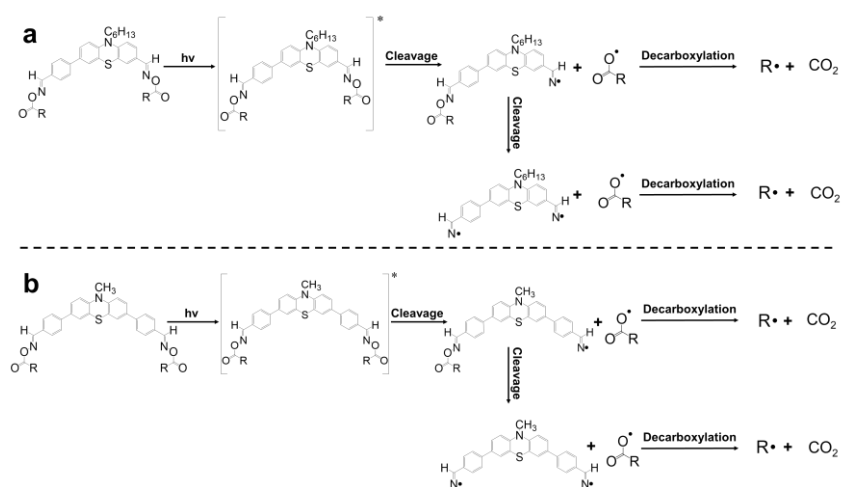


Figure 6. ESR-ST spectra of the radical adducts of (a) and (b) OXE-A1, (c) and (d) OXE-B2, and (e) and (f) PXE-B4 under LED@405 nm irradiation in tert-butylbenzene.

Photoinitiation Mechanism

Based on the above results, the proposed mechanism for photoinitiation is shown in Scheme 3. According on the light exposure, OXEs can be promoted in the excited state, so that iminyl and acyloxy/aryloxy radicals are generated from the dissociation of the N-O bond of OXEs (the cleavage reaction). Furthermore, acyloxy/aryloxy radicals can produce the active free radicals and CO₂ through decarboxylation reaction.



Scheme 3. Proposed Photoinitiation Mechanism of (a) series OXE-A and (b) series OXE-B.

3D Printing

In order to explore the application of OXE/TMPTA system in 3D printing, OXE-A1/TMPTA, OXE-B2/TMPTA and OXE-B4/TMPTA were used as a model system to carry out 3D printing with a stereolithography (SLA) printer, according to the favorable photoinitiation performance in TMPTA photopolymerization. The printing conditions were optimized in that prototypes of 3D structures were printed on the SLA 3D printer, with the curing parameter controlled by software. As shown in Figure 7, 3D printed chesses were successfully printed, and the top parts are clearly visible. However, 3D structure based on OXE-B2/TMPTA could not be manufactured successfully, despite the printing conditions were optimized. Then, direct laser write (DLW) was performed on OXE-B2/TMPTA, and two thin objects (thickness 0.5 mm) in Figure 7 c were obtained within a short time (around 2 min) (see Figure 7.c).

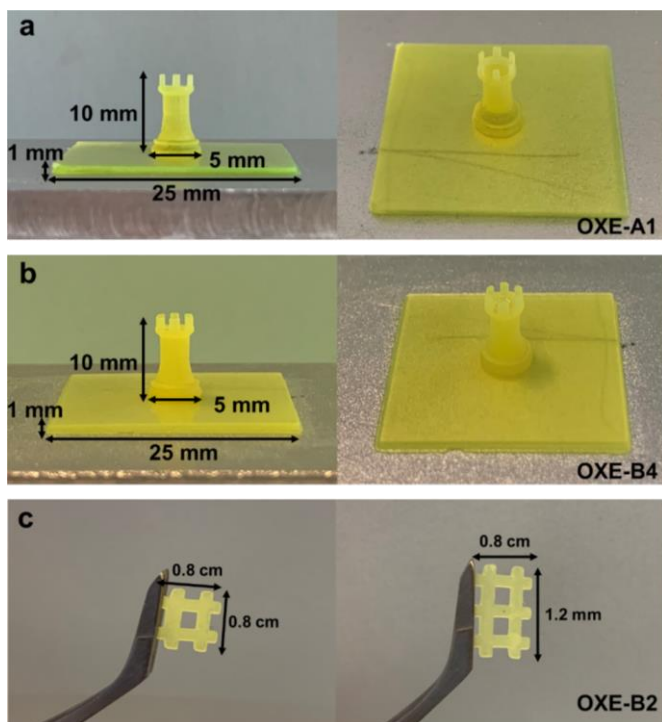


Figure 7. Digital photos of 3D printed objects using (a) OXE-A1/TMPTA and (b) OXE-B4 respectively.

Thermal Initiation Behavior

Normally, free radicals in OXEs polymerization systems can also be generated by thermal degradation. DSC thermograms of OXE-A0, OXE-A1, OXE-B0, OXE-B2 and OXE-B4 in TMPTA are shown in Figure 8 and their parameters (T_{initial} , T_{max} and the final acrylate conversion of TMPTA) are listed in Table 6. T_{initial} values of OXE-A0 and OXE-B0 in TMPTA are both above 130°C and their conversions are 27.5% and 29.9% respectively. All of the analyzed oxime esters have lower T_{initial} values and higher conversions. Interestingly, OXE-A1, OXE-B2 and OXE-B4 show the dual photo/thermal initiation behavior, which can for example be used for the preparation of carbon fiber composites which are non-transparent and can only be cured thermally or by dual, light plus thermal activation.

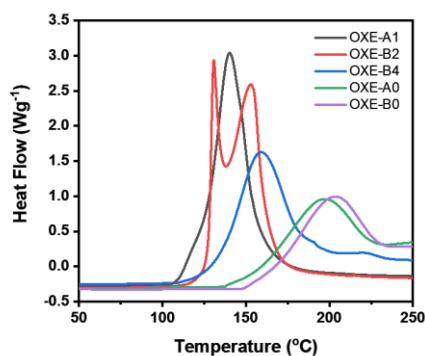


Figure 8. DSC thermograms of OXEs in TMPTA. **The presence of oxime esters (OXE-A1, OXE-B2, OXE-B4) clearly moves the decomposition to lower temperatures.**

Table 6. Parameters about thermal polymerization.

Pis (10^{-5} mol/g)	T _{initial} (°C)	T _{max} (°C)	Conversion (%)
OXE-A1	85.0	141.6	63.4
OXE-B2	83.7, 123.2	132.6, 154.3	51.4
OXE-B4	98.8	159.7	49.3
OXE-A0	130.5	195.2	27.5
OXE-B0	145.1	201.8	29.9

Conclusion

Twelve phenothiazines containing two oxime ester functionalities as terminal groups were designed and synthesized. Through theoretical calculations, all of these photoinitiators have the ability for photoinitiation. OXE-A1, OXE-B2 and OXE-B4 exhibit good efficient light absorptivity and efficient photolysis performance under the irradiation of 405 nm LED. $\Delta H_{\text{cleavage } S1} < 0$ and $\Delta H_{\text{cleavage } T1} < 0$ both indicate the favorable cleavage process from singlet excited-state or triplet excited-state. These three OXEs demonstrate better performance than the commercial photoinitiator TPO, and OXE-A1 and OXE-B4 based formulations can be used to print 3D objects *via* SLA. In addition, dual photo/thermal behavior also can be observed for these three OXEs. Investigation of the mechanism of these OXEs indicates the generation of the acyloxy

and iminyl radicals from N-O bond cleavage process, followed by a decarboxylation reaction of the acyloxy radicals resulting in active radicals and CO₂. The active radicals can induce the free radical photopolymerization of TMPTA. According to the literature, the iminyl radical is also reactive. In this work, these OXEs can initiate photopolymerization with a low concentration (1×10^{-5} mol g⁻¹ in TMPTA, or 0.45 wt% to 0.76 wt% depending on their different molecular masses), which fully demonstrate the initiation ability of these compounds containing two oxime esters. Therefore, this work exhibits the significance of type 1 photoinitiators containing two oxime esters functionalities and provides a strategy for the development of novel oxime ester-based photoinitiators with high performance.

ASSOCIATED CONTENT

Supporting Information. HOMO and LUMO orbits of the series OXE-A at the uB3LYP/6-31G* level (iso-value = 0.02) (Scheme S1), HOMO and LUMO orbits of the series OXE-B (from OXE-B0 to OXE-B4) at the uB3LYP/6-31G* level (iso-value = 0.02) (Scheme S2), HOMO and LUMO orbits of the series OXE-B (from OXE-B5 to OXE-B9) at the uB3LYP/6-31G* level (iso-value = 0.02) (Scheme S3), UV-visible absorption spectra of OXEs in acetonitrile (Figure S1), Images of acetonitrile solvents containing OXE-A1- OXE-A3 respectively (Figure S2), Images of acetonitrile solvents containing OXE-B1-OXE-B9 respectively (Figure S3), Steady-state photolysis of OXE-A2 and OXE-A3 in acetonitrile upon the irradiation of 405 nm LED (Figure S4), Steady-state photolysis of OXE-B1-OXEB3 and OXE-B5-OXE-B9 in acetonitrile upon the irradiation of 405 nm LED (Figure S5), Singlet-state energy determination of OXE-A0, OXE-A2 and OXE-A3 (Figure S6), Singlet-state energy determination of OXE-B0-OXE-B3 and OXE-B5-OXE-B9 (Figure S7), Figure S8 Fluorescence decay curve of OXE-A0, OXE-A2 and OXE-A3 (Figure S8), Fluorescence decay curve of OXE-B0-OXE-B3 and OXE-B5-OXE-B9 (Figure S9), Photopolymerization profiles of TMPTA in laminate (1.4 mm) upon exposure to 405 nm LED in the presence of different OXEs (1×10^{-5} mol g⁻¹ in TMPTA) (Figure S10), Infrared spectra of TMPTA containing OXE-A0, OXE-A2 and OXE-A3 respectively at t = 10 and 30 s (Figure S11), Infrared spectra of TMPTA containing B0-OXE-B3 and OXE-B5-OXE-B9

respectively at $t = 10$ and 30 s (Figure S12), The absorption intensity of CO_2 obtained from the OXE-A2/TMPTA, OXE-A3/TMPTA, OXE-B2/TMPTA, OXE-B3/TMPTA, OXE-B7/TMPTA and OXE-B8/TMPTA systems respectively (Figure S13), Picture of the formulation containing OXE-B1 (1×10^{-5} mol g^{-1} in TMPTA). (Figure S14), General Information of OXEs Syntheses.

AUTHOR INFORMATION

Corresponding Author

Jacques Lalevée, Université de Haute-Alsace, CNRS, IS2M UMR 7361, F-68100 Mulhouse, France; Université de Strasbourg, France; E-mail : jacques.lalevee@uha.fr

Fabrice Morlet-Savary, Université de Haute-Alsace, CNRS, IS2M UMR 7361, F-68100 Mulhouse, France; Université de Strasbourg, France; E-mail : fabrice.morlet-savary@uha.fr

Frédéric Dumur, Aix Marseille Univ, CNRS, ICR, UMR 7273, F-13397 Marseille, France; E-mail : frederic.dumur@univ-amu.fr

Funding

The authors thank the Region Grand Est (France) for the grant “MIPPI-4D” and the Agence Nationale de la Recherche for fundings provided by the ANR PhotoFlat.

Author Contributions

The manuscript was written through contributions of all authors. All authors have given approval to the final version of the manuscript.

Notes

The authors declare no competing financial interest. The raw/processed data required to reproduce these findings can be furnished on demand.

ABBREVIATIONS

PI, photoinitiator; OXE, oxime ester; TPO, diphenyl(2,4,6-trimethylbenzoyl)phosphine oxide; LEDs, light-emitting diodes; ZnO, zinc oxide; ESR-ST, electron spin resonance spin trapping; TMPTA, trimethylolpropane triacrylate; FRP, free radical photopolymerization; PBN, N-tert-Butyl- α -phenylnitron; IRF, impulse response function; E_{S1} , singlet excited-state energies; E_{T1} , triplet excited states; S_1 , singlet excited states; T_1 , triplet excited states; $\Delta H_{\text{Cleavage}}$, enthalpies of the cleavage process of

the N-O bond; BDE, the dissociation energies of the N-O bond; RT-FTIR, real-time Fourier transformed infrared; FC, final conversion; λ_{\max} , the maximum wavelength of absorption; ϵ_{\max} , the molar extinction coefficients at maximum absorption wavelength; $\epsilon_{405\text{nm}}$, the molar extinction coefficients at 405 nm; SLA, stereolithography; DLW, direct laser write; HOMO, Highest Occupied Molecular Orbital; LUMO, Lowest Unoccupied Molecular Orbitals; $\Delta H_{\text{decarboxylation}}$, enthalpy of decarboxylation reaction;

References

1. Zhang, F.; Zhu, L.; Li, Z.; Wang, S.; Shi, J.; Tang, W.; Li, N.; Yang, J., The Recent Development of Vat Photopolymerization: A Review. *Addit. Manuf.* **2021**, *48*, 102423-102442.
2. Tasdelen, M. A.; Lalevée, J.; Yagci, Y., Photoinduced free radical promoted cationic polymerization 40 years after its discovery. *Polym. Chem.* **2020**, *11* (6), 1111-1121.
3. Mokbel, H.; Graff, B.; Dumur, F.; Lalevee, J., NIR sensitizer operating under long wavelength (1064 nm) for free radical photopolymerization processes. *Macromol. Rapid Comm.* **2020**, *41* (15), 2000289-2000293.
4. Zhao, X.; Zhao, Y.; Li, M.-D.; Li, Z. a.; Peng, H.; Xie, T.; Xie, X., Efficient 3D Printing via Photooxidation of Ketocoumarin Based Photopolymerization. *Nat. Commun.* **2021**, *12* (1), 2873-2880.
5. Zhang, Y.; Xu, Y.; Simon-Masseron, A.; Lalevee, J., Radical Photoinitiation with LEDs and Applications in the 3D Printing of Composites. *Chem Soc Rev* **2021**, *50* (6), 3824-3841.
6. Bagheri, A.; Jin, J., Photopolymerization in 3D Printing. *ACS Appl. Polym. Mater.* **2019**, *1* (4), 593-611.
7. Dietlin, C.; Schweizer, S.; Xiao, P.; Zhang, J.; Morlet-Savary, F.; Graff, B.; Fouassier, J.-P.; Lalevée, J., Photopolymerization upon LEDs: New photoinitiating Systems and Strategies. *Polym. Chem.* **2015**, *6* (21), 3895-3912.
8. Corrigan, N.; Yeow, J.; Judzewitsch, P.; Xu, J.; Boyer, C., Seeing the Light: Advancing Materials Chemistry through Photopolymerization. *Angew. Chem. Int. Ed. Engl.* **2019**, *58* (16), 5170-5189.

9. Yeow, J.; Chapman, R.; Gormley, A. J.; Boyer, C., Up in the air: oxygen tolerance in controlled/living radical polymerisation. *Chem Soc Rev* **2018**, *47* (12), 4357-4387.

10. Li, J.; Zheng, H.; Lu, H.; Li, J.; Yao, L.; Wang, Y.; Zhou, X.; Nie, J.; Zhu, X.; Fu, Z., Study on Pyrrole Chalcone Derivatives Used for Blue LED Free Radical Photopolymerization: Controllable Initiating Activity Achieved through Photoisomerization Property. *Eur. Polym. J.* **2022**, *176*, 111393-111400.

11. Jandt, K. D.; Mills, R. W., A Brief History of LED Photopolymerization. *Dent. Mater.* **2013**, *29* (6), 605-617.

12. Guo, X.; Mao, H.; Bao, C.; Wan, D.; Jin, M., Fused Carbazole–Coumarin–Ketone Dyes: High Performance and Photobleachable Photoinitiators in Free Radical Photopolymerization for Deep Photocuring under Visible LED Light Irradiation. *Polym. Chem.* **2022**, *13* (22), 3367-3376.

13. Liu, S.; Brunel, D.; Noirbent, G.; Mau, A.; Chen, H.; Morlet-Savary, F.; Graff, B.; Gigmes, D.; Xiao, P.; Dumur, F.; Lalevée, J., New multifunctional benzophenone-based photoinitiators with high migration stability and their applications in 3D printing. *Mater. Chem. Front.* **2021**, *5* (4), 1982-1994.

14. Chen, H.; Noirbent, G.; Liu, S.; Brunel, D.; Graff, B.; Gigmes, D.; Zhang, Y.; Sun, K.; Morlet-Savary, F.; Xiao, P.; Dumur, F.; Lalevée, J., Bis-chalcone derivatives derived from natural products as near-UV/visible light sensitive photoinitiators for 3D/4D printing. *Mater. Chem. Front.* **2021**, *5* (2), 901-916.

15. Ma, X.; Cao, D.; Fu, H.; You, J.; Gu, R.; Fan, B.; Nie, J.; Wang, T., Multicomponent photoinitiating systems containing arylamino oxime ester for visible light photopolymerization. *Prog. Org. Coat.* **2019**, *135*, 517-524.

16. Hammoud, F.; Hijazi, A.; Duval, S.; Lalevée, J.; Dumur, F., 5,12-Dihydroindolo[3,2-a]carbazole: A Promising Scaffold for the Design of Visible Light Photoinitiators of Polymerization. *Eur. Polym. J.* **2022**, *162*, 110880-110891.

17. Liu, S.; Brunel, D.; Noirbent, G.; Mau, A.; Chen, H.; Morlet-Savary, F.; Gigmes, D.; Xiao, P.; Dumur, F.; Lalevée, J., New Multifunctional Benzophenone-

based Photoinitiators with High Migration Stability and the Application in 3D Printing. *Mater. Chem. Front.* **2021**, *5* (4), 1982-1994.

18. Sun, K.; Xu, Y.; Dumur, F.; Morlet-Savary, F.; Chen, H.; Dietlin, C.; Graff, B.; Lalevée, J.; Xiao, P., In silico rational design by molecular modeling of new ketones as photoinitiators in three-component photoinitiating systems: Application in 3D printing. *Polym. Chem.* **2020**, *11* (12), 2230-2242.

19. Li, Z.; Zou, X.; Zhu, G.; Liu, X.; Liu, R., Coumarin-Based Oxime Esters: Photobleachable and Versatile Unimolecular Initiators for Acrylate and Thiol-Based Click Photopolymerization under Visible Light-Emitting Diode Light Irradiation. *ACS Appl. Mater. Inter* **2018**, *10* (18), 16113-16123.

20. Schmitt, M., Synthesis and testing of ZnO nanoparticles for photo-initiation: Experimental observation of two different non-migration initiators for bulk polymerization. *Nanoscale* **2015**, *7* (21), 9532-44.

21. Schmitt, M., ZnO Nanoparticle Induced Photo-Kolbe Reaction, Fragment Stabilization and Effect on Photopolymerization Monitored by Raman-UV-Vis Measurements. *Macromol. Chem. Phys.* **2012**, *213* (18), 1953-1962.

22. Pang, Y.; Fan, S.; Wang, Q.; Oprych, D.; Feilen, A.; Reiner, K.; Keil, D.; Slominsky, Y. L.; Popov, S.; Zou, Y.; Strehmel, B., NIR-Sensitized Activated Photoreaction between Cyanines and Oxime Esters: Free-Radical Photopolymerization. *Angew. Chem. Int. Ed. Engl.* **2020**, *59* (28), 11440-11447.

23. Qiu, W.; Li, M.; Yang, Y.; Li, Z.; Dietliker, K., Cleavable Coumarin-Based Oxime Esters with Terminal Heterocyclic Moieties: Photobleachable Initiators for Deep Photocuring under Visible LED Light Irradiation. *Polym. Chem.* **2020**, *11* (7), 1356-1363.

24. Wu, X.; Gong, S.; Chen, Z.; Hou, J.; Liao, Q.; Xiong, Y.; Li, Z.; Tang, H., Photobleachable Bis-Chalcones-Based Oxime Ester Dyes for Radical Visible Photopolymerization. *Dyes Pigm.* **2022**, *205*, 110556-111565.

25. Dumur, F., Recent Advances on Carbazole-based Oxime Esters as Photoinitiators of Polymerization. *Eur. Polym. J.* **2022**, *175*, 111330-111360.

26. Yin, W.; Wang, X., Recent Advances in Iminyl Radical-Mediated Catalytic Cyclizations and Ring-Opening Reactions. *New J. Chem.* **2019**, *43* (8), 3254-3264.

27. Wang, W.; Jin, M.; Pan, H.; Wan, D., Phenylthioether Thiophene-Based Oxime Esters as Novel Photoinitiators for Free Radical Photopolymerization under LED Irradiation Wavelength Exposure. *Prog. Org. Coat.* **2021**, *151*, 106019-106030.

28. Fast, D. E.; Lauer, A.; Menzel, J. P.; Kelterer, A.-M.; Gescheidt, G.; Barner-Kowollik, C., Wavelength-Dependent Photochemistry of Oxime Ester Photoinitiators. *Macromolecules* **2017**, *50* (5), 1815-1823.

29. Liu, S.; Giacometto, N.; Schmitt, M.; Nechab, M.; Graff, B.; Morlet-Savary, F.; Xiao, P.; Dumur, F.; Lalevée, J., Effect of Decarboxylation on the Photoinitiation Behavior of Nitrocarbazole-Based Oxime Esters. *Macromolecules* **2022**, *55* (7), 2475-2485.

30. Lee, Z.-H.; Hammoud, F.; Hijazi, A.; Graff, B.; Lalevée, J.; Chen, Y.-C., Synthesis and Free Radical Photopolymerization of Triphenylamine-Based Oxime Ester Photoinitiators. *Polym. Chem.* **2021**, *12* (9), 1286-1297.

31. Hammoud, F.; Giacometto, N.; Noirbent, G.; Graff, B.; Hijazi, A.; Nechab, M.; Gignes, D.; Dumur, F.; Lalevée, J., Substituent Effects on Photoinitiation Ability of Coumarin-Based Oxime-Ester Photoinitiators for Free Radical Photopolymerization. *Mater. Chem. Front.* **2021**, *5* (24), 8361-8370.

32. Lee, Z. H.; Yen, S. C.; Hammoud, F.; Hijazi, A.; Graff, B.; Lalevee, J.; Chen, Y. C., Naphthalene-Based Oxime Esters as Type I Photoinitiators for Free Radical Photopolymerization. *Polymers* **2022**, *14* (23).

33. Zhou, R.; Pan, H.; Wan, D.; Malval, J.-P.; Jin, M., Bicarbazole-Based Oxime Esters as Novel Efficient Photoinitiators for Photopolymerization under UV-Vis LEDs. *Prog. Org. Coat.* **2021**, *157*, 106306-106314.

34. Ding, Y.; Jiang, S.; Gao, Y.; Nie, J.; Du, H.; Sun, F., Photochromic Polymers Based on Fluorophenyl Oxime Ester Photoinitiators as Photoswitchable Molecules. *Macromolecules* **2020**, *53* (14), 5701-5710.

35. Lee, W. J.; Kwak, H. S.; Lee, D.-r.; Oh, C.; Yum, E. K.; An, Y.; Halls, M. D.; Lee, C.-W., Design and Synthesis of Novel Oxime Ester Photoinitiators Augmented by Automated Machine Learning. *Chem. Mater.* **2021**, *34* (1), 116-127.

36. Chen, S.; Jin, M.; Malval, J.-P.; Fu, J.; Morlet-Savary, F.; Pan, H.; Wan, D., Substituted Stilbene-Based Oxime Esters Used as Highly Reactive Wavelength-Dependent Photoinitiators for LED Photopolymerization. *Polym. Chem.* **2019**, *10* (48), 6609-6621.

37. Wang, W.; Jin, M.; Pan, H.; Wan, D., Remote effect of substituents on the properties of phenyl thienyl thioether-based oxime esters as LED-sensitive photoinitiators. *Dyes Pigm.* **2021**, *192*.

38. Hammoud, F.; Giacoletto, N.; Nechab, M.; Graff, B.; Hijazi, A.; Dumur, F.; Lalevée, J., 5,12-Dialkyl-5,12-dihydroindolo[3,2- a]carbazole-Based Oxime-Esters for LED Photoinitiating Systems and Application on 3D Printing. *Macromol. Mater. Eng.* **2022**, *307* (8), 2200082-2200091.

39. Dietlin, C.; Trinh, T. T.; Schweizer, S.; Graff, B.; Morlet-Savary, F.; Noirot, P.-A.; Lalevée, J., Rational design of acyldiphenylphosphine oxides as photoinitiators of radical polymerization. *Macromolecules* **2019**, *52* (20), 7886-7893.

40. Liu, S.; Giacoletto, N.; Graff, B.; Morlet-Savary, F.; Nechab, M.; Xiao, P.; Dumur, F.; Lalevée, J., N-Naphthalimide Ester Derivatives as Type I Photoinitiators for LED Photopolymerization. *Mater. Today Chem.* **2022**, *26*, 101137-101145.